

Article

Analysis of Drought-Sensitive Areas and Evolution Patterns through Statistical Simulations of the Indian Ocean Dipole Mode

Qing-Gang Gao ¹, Vonevilay Sombutmounvong ¹, Lihua Xiong ¹ , Joo-Heon Lee ²  and Jong-Suk Kim ^{1,*} 

¹ State Key Laboratory of Water Resources and Hydropower Engineering Science, Wuhan University, Wuhan 430072, China; 2014301580312@whu.edu.cn (Q.-G.G.); vonevilay12345@gmail.com (V.S.); xionglh@whu.edu.cn (L.X.)

² Department of Civil Engineering, Joongbu University, Go Yang, Gyeong Gi 10279, Korea; leejh@joongbu.ac.kr

* Correspondence: jongsuk@whu.edu.cn

Received: 13 May 2019; Accepted: 20 June 2019; Published: 23 June 2019



Abstract: In this study, we investigated extreme droughts in the Indochina peninsula and their relationship with the Indian Ocean Dipole (IOD) mode. Areas most vulnerable to drought were analyzed via statistical simulations of the IOD based on historical observations. Results of the long-term trend analysis indicate that areas with increasing spring (March–May) rainfall are mainly distributed along the eastern coast (Vietnam) and the northwestern portions of the Indochina Peninsula (ICP), while Central and Northern Laos and Northern Cambodia have witnessed a reduction in spring rainfall over the past few decades. This trend is similar to that of extreme drought. During positive IOD years, the frequency of extreme droughts was reduced throughout Vietnam and in the southwestern parts of China, while increased drought was observed in Cambodia, Central Laos, and along the coastline adjacent to the Myanmar Sea. Results for negative IOD years were similar to changes observed for positive IOD years; however, the eastern and northern parts of the ICP experienced reduced droughts. In addition, the results of the statistical simulations proposed in this study successfully simulate drought-sensitive areas and evolution patterns of various IOD changes. The results of this study can help improve diagnostic techniques for extreme droughts in the ICP.

Keywords: extreme drought; Indochina Peninsula; Indian Ocean Dipole; intentionally biased bootstrap method

1. Introduction

Since the 1950s, an increase in atmospheric moisture demand and changes in atmospheric circulation patterns due to global warming have contributed to increased aridity in many areas [1,2]. Furthermore, drought risk in the twenty-first century, indicated by model-simulated drought indices [3] and soil moisture [4], is expected to increase.

Drought is often divided into four types [5]: meteorological or climatological, agricultural, hydrological, and socio-economic. Of these four types, we chose to analyze meteorological drought because this type of drought results in water shortages due to reduced rainfall [6]. To better anticipate drought-related disasters in Southeast Asia, we studied the Indochina Peninsula (ICP). Several studies focusing on the impacts of droughts have been conducted in the ICP. Recently, Le et al. [7] attempted to ascertain the relationship between meteorological drought in the Khánh Hòa Province (Vietnam) and climate signals, such as the Southern Oscillation Index and the Bivariate El Niño Southern Oscillation (ENSO) time series. Their work shed light on the importance of climate signals of oceanic and

atmospheric circulations in forecasting meteorological drought. However, little attention has been paid to drought mitigation in this area [7–10].

An international Drought Management Program has been implemented by the Mekong River Commission Secretariat for the Mekong River Basin. It aims to demonstrate the social impacts of increased mitigation measures for droughts in the area [9]. To obtain a comprehensive view on drought assessments, climate projections under different scenarios have also been used for a river basin in the Vietnamese central highlands, an important area for coffee production and generating hydropower [10]. Herein, the importance of the regional climate model in investigations of water supply and water balance in the region for future planning and adaptation has been highlighted. To improve rice yield, Shu et al. [11] studied drought in Thailand and Laos, which are prone to early- and late-season droughts, both of which have strong negative influences on crop yields in this region. It was proposed that crop losses due to limited water supplies can be effectively reduced by using more drought-resistant cultivars, applying appropriate fertilizers, and controlling sowing time.

To improve the predictability of droughts, their relationship with climate signals has been widely investigated [6,12,13]. The Indian Ocean Dipole (IOD) mode represents anomalous and strong zonal Sea Surface Temperature (SST) gradients in the tropical Indian Ocean (TIO), which has a distinct dipole structure [14]. During the positive phase of the IOD, above-normal SST and precipitation are observed in the Western Indian Ocean, while cooling and drying phenomena are dominant in the Eastern Indian Ocean. The opposite is true during the negative phase. The impact of the IOD on SST is consistent with that of rainfall over the central equatorial Indian Ocean. Wind anomalies induced by the IOD can significantly enhance the SST difference and alter the thermocline in the Indian Ocean as positive feedback, which is similar to the effects of the ENSO on the tropical Pacific [14,15]. Similarity between the IOD and the ENSO and their strong local coupling mechanism have attracted significant research attention [16,17], and because of this, the remote impacts of the IOD on ocean climate have been widely detected.

To understand the global impacts of the IOD in detail, Saji et al. [18] examined its influence on global temperature and precipitation independent of the ENSO. A strong correlation was found between the IOD and rainfall and temperature across Europe, Northeastern Asia, America, and South Africa. The impacts of the IOD on Australian [19–21] and South America rainfall [22] have also been investigated. The anomalously cool SST of the Eastern Indian Ocean, induced by the positive phase of the IOD, causes anomalous anticyclonic circulation over the Australian continent, which reduces rainfall [19]. Inter-annual precipitation variability in Brazil also appears to be influenced by the IOD through a mid-latitude wave train. Positive correlation between spatially averaged North Atlantic and Indian Ocean SSTs might suggest a complex mechanism between the IOD and regional precipitation [23]. Although the frequencies of the positive and negative IODs are not projected to change, a decrease in the difference in magnitude between them is expected [24], which might have impacts on the regional climate. An investigation of IOD events from 1880 to 2004 revealed a link between the occurrence of intense and frequent positive IODs and regional climate [25].

This study aimed to improve drought prediction in the ICP, whose correlation with IOD has not been investigated in detail. To this end, spring precipitation and extreme drought changes caused by ocean warming in the Indo-Pacific region were analyzed. In addition, the IOD-sensitive hotspots for extreme droughts in the ICP were identified using an intentionally biased bootstrap (IBB) approach based on statistical simulations of observational data to determine drought predictability. Moreover, trends in spatio-temporal variations in seasonal precipitation and extreme droughts in the ICP were identified because the analysis of this trend will help in future predictions of droughts in the area by improving our understanding of local climate variabilities.

2. Data and Methods

This study used the high-resolution ($0.5^\circ \times 0.5^\circ$) daily Climate Prediction Center Global Unified Precipitation data for a period of 40 years (1979–2018) provided by the National Oceanic and

Atmospheric Administration Earth System Research Laboratory, Boulder, Colorado, USA, to identify spring (March–May) precipitation variability over the ICP region, which consists of six countries: Myanmar, Thailand, Laos, Cambodia, Vietnam, and Malaysia (Figure 1). For extraction of two types of El Niño events, a simple transformation proposed by Ren and Jin [26] was applied using the Niño 3 and Niño 4 indices. To classify the IOD events, we used the monthly SST data obtained from the National Oceanic and Atmospheric Administration in the TIO region. The three-month running average was applied to the peak phase of the IOD mode during August–October, with $\pm 1\sigma$ (standard deviation) to identify positive and negative patterns of the IODs. Finally, 12 events (1961, 1963, 1967, 1972, 1977, 1982, 1994, 1997, 2006, 2012, 2015, and 2017) and 11 events (1954, 1958, 1960, 1964, 1971, 1975, 1989, 1992, 1996, 1998, and 2010) were selected as the strongest positive IOD years and negative IOD years, respectively. The selected IOD years were used for composite analysis to investigate changes in the long-term mean (1981–2010) of seasonal precipitation and extreme drought in the ICP.

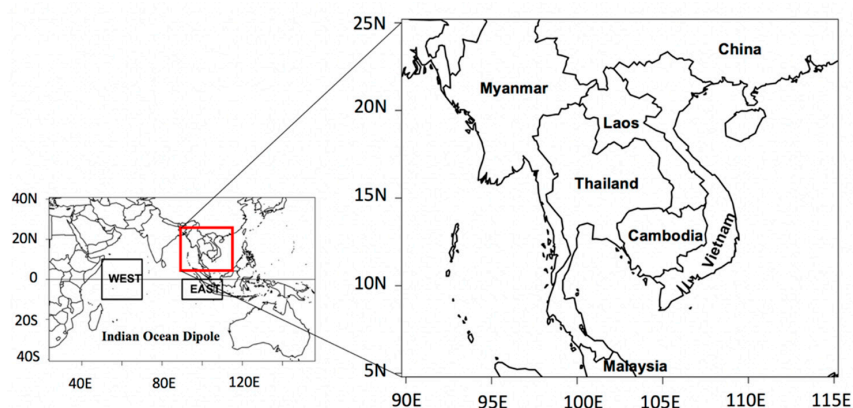


Figure 1. Indochina Peninsula (90° E–115° E, 5° N–25° N). The Indian Ocean Dipole (IOD) mode is defined as the difference in the sea surface temperature between the western (10° S–10° N, 50°–70° E) and southeastern region (10° S to the equator, 90°–110° E) of the tropical Indian Ocean, shown on the left panel.

In this study, the Standardized Precipitation Index (SPI) [27] was adopted to extract drought information on a daily basis for each drought duration, using precipitation data from 1979–2018. During the calculation of the SPI, n-day precipitation data was aggregated after each day from March 1 to May 31 to obtain the probability fitted to the gamma distribution, which was then converted to a standardized normal distribution with a mean of 0 and a standard deviation of 1 [28]. In this study, the extreme drought is defined as the number of drought events occurring during March–May by applying a -1.5 threshold to the SPI calculated on a 30-day basis. The technique of approximate conversion that transforms the cumulative probability of precipitation into a standardized variable Z was developed by McKee et al. [27].

$$\text{SPI} = Z = \begin{cases} -\left(t - \frac{c_0 + c_1 t + c_2 t^2}{1 + d_1 t + d_2 t^2 + d_3 t^3}\right), & \text{for } 0 < H(x) \leq 0.5, \\ +\left(t - \frac{c_0 + c_1 t + c_2 t^2}{1 + d_1 t + d_2 t^2 + d_3 t^3}\right), & \text{for } 0.5 < H(x) < 1. \end{cases} \quad (1)$$

where

$$c_0 = 2.515517, \quad c_1 = 0.802853, \quad c_2 = 0.010328, \\
 d_0 = 1.432788, \quad d_1 = 0.189269, \quad d_2 = 0.001308.$$

$$t = \begin{cases} \sqrt{\ln\left[\frac{1}{(H(x))^2}\right]}, & \text{for } 0 < H(x) \leq 0.5, \\ \sqrt{\ln\left[\frac{1}{(1-H(x))^2}\right]}, & \text{for } 0.5 < H(x) < 1. \end{cases} \quad (2)$$

where x is precipitation, and $H(x)$ is the cumulative probability of the observed precipitation.

Trend testing aims to specify whether an increasing or decreasing trend exists in time series data. Since parametric tests require several assumptions involving normality, stationarity, and/or independence of variables, non-parametric methods are preferred in meteorological and hydrological studies. One of the widely used nonparametric trend tests is the Mann–Kendall (M–K) test [29,30]. Herein, we adopted a modified M–K test to consider autocorrelation in time-series data [31]. The accuracy of the modified M–K test was significantly improved by using autocorrelated data to test the null hypothesis (H_0) that no trend exists in the sample data. Using the modified M–K test, we classified the confidence levels of the trends for the 90% and 95% intervals. In this study, trend analysis was performed to identify spatio-temporal variations in seasonal precipitation and extreme droughts in the ICP.

The Intentionally Biased Bootstrapping (IBB) method was developed by Hall and Presnell [32] to adjust a “uniform” bootstrap by reducing bias or variance, or by setting some characteristics as predetermined quantities. The IBB method makes it possible to apply the nonlinear relationship between two parameters as the resampling probability to predict one of the parameters. Using the IBB method, the change in the mean of the predicted parameter can be estimated according to the change in the mean of the base parameter. Recently, Lee [33] employed the IBB method to assess the impact of regional temperature on rainfall based on historical data before evaluating future changes in the global warming scenarios of seasonal rainfall over the Korean Peninsula. The IBB approach can assess the impact of rainfall as temperatures increase with the current climate horizon. Thus, the IBB method is suitable for determining the sensitivity of regional rainfall with changes in SST in the Indian Ocean.

Briefly, after obtaining expected increase or decrease ($\Delta\mu$) of the mean of the base parameter, we resampled the parameter pairs with weights based on the sequence of the base parameter (arranged from small to large) as follows:

$$S_{i,n}^r = (i/n)^r \quad (3)$$

where n is the number of parameter pairs, $i = 1, \dots, n$, and the weight order (r) is used to generalize the weights. Then, using the equation below, we estimated r , and hence the resample weights.

$$\Delta\mu = \frac{1}{\psi_r} \sum_{i=1}^n S_{i,n}^r x_i - \frac{1}{n} \sum_{i=1}^n x_i \quad (4)$$

where $\psi_r = \sum_{i=1}^n S_{i,n}^r$

3. Results of the Analysis

3.1. Trends in Spring Precipitation and Extreme Drought

Trends in precipitation during spring (March–May) and extreme drought (1979–2017) in the ICP are depicted in Figure 2. As shown in Figure 2a, the regions exhibiting increased spring rainfall are mainly distributed along the east coast (Vietnam) and the northwest regions of the ICP, while central and Northern Laos and Northern Cambodia experienced a decrease in spring precipitation during the past four decades. This trend is similar to that of the extreme drought shown in Figure 2b, in which Vietnam experienced fewer extreme droughts while the central and northern parts of Laos suffered more extreme droughts. The increasing trend in extreme droughts appears across the ICP, except for Vietnam, but this is not statistically significant.

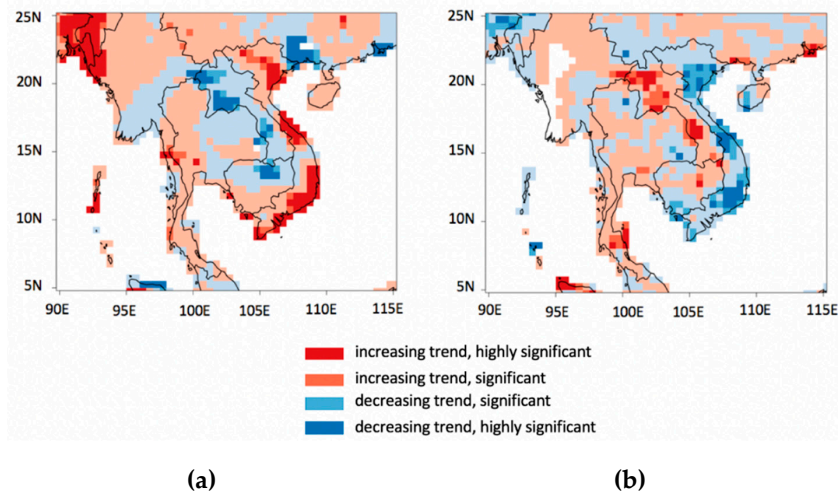


Figure 2. Trends in (a) spring precipitation and (b) extreme drought in the Indochina Peninsula. The modified Mann–Kendall (M–K) test was applied; statistically significant changes are highlighted in red (increasing trend) and blue (decreasing trend) for 90% (significant) and 95% (highly significant) confidence intervals.

3.2. Composite Anomaly of Extreme Drought for IOD Modes

Figure 3 shows the composite anomalies of extreme drought during the spring season (March–May) for positive and negative IOD years. During the positive IOD years, negative anomaly patterns of drought were dominant throughout Vietnam and the southwestern region of the Yunnan Province in China. However, a positive anomaly became evident over central Cambodia and Laos, with distinct abnormalities occurring along the coastline adjacent to the Myanmar Sea; in some areas, abnormalities recorded were more than 160% higher than usual. Furthermore, if both positive IOD years and El Niño events occurred simultaneously, the spatial distribution of extreme drought was observed to intensify only compared to drought anomaly patterns during the positive IOD years. The change in extreme drought during negative IOD years was similar to the change in positive IOD years. Positive anomaly of extreme drought around Myanmar’s coastline was weakened, and positive anomalies were more evident across Cambodia. The results for negative IOD years were similar to the changes for positive IOD years; however, the anomalies increased towards Northern Laos, Northeastern Myanmar, and Northern Thailand. These changes were more evident when the negative IOD years coincided with La Niña events.

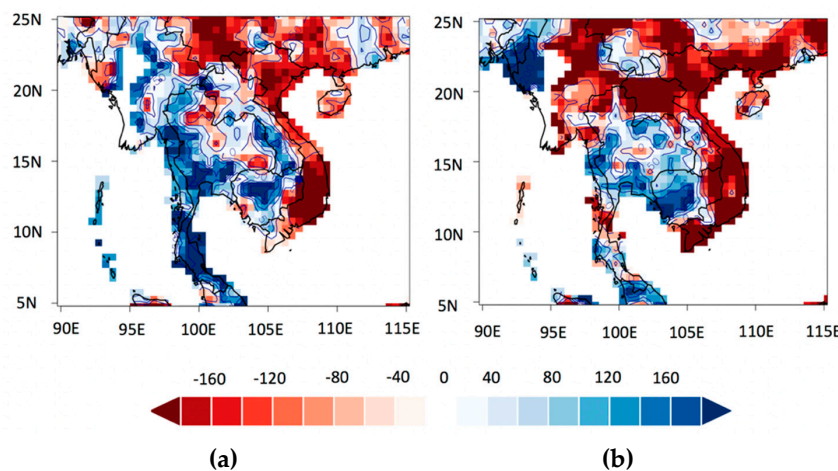


Figure 3. Percentage composite anomalies in extreme drought (departures from the 1981–2010 norms) during (a) positive IOD years and (b) negative IOD years.

3.3. Changes in Extreme Drought Using the IBB method

Figures 4 and 5 show the results of composite anomalies of extreme drought (shown as a percentage of the normal) during spring in relation to positive and negative IOD simulations over the ICP. An increase of 0.25σ in IOD (Figure 4) resulted in more extreme drought across Laos and along the coastline adjacent to the Myanmar Sea, and less extreme droughts than usual across Southern Cambodia, Vietnam, and Northwest Myanmar, adjacent to the Bay of Bengal. As IOD increases, drought changes appear more severe. The northwestern region of Myanmar was observed to have a statistically significant increase in extreme drought for more than 0.5σ of the IOD. Some parts of Southern Thailand and Western Cambodia showed a statistically significant negative anomaly pattern of extreme drought. These patterns tended to be reinforced when drought symptoms appeared from $+0.75\sigma$ to $+1\sigma$ of the IOD. In addition, statistically significant patterns of positive anomalies in extreme droughts in some areas along the coastline of the Myanmar Sea were observed in cases of more than $+1\sigma$ of IOD changes.

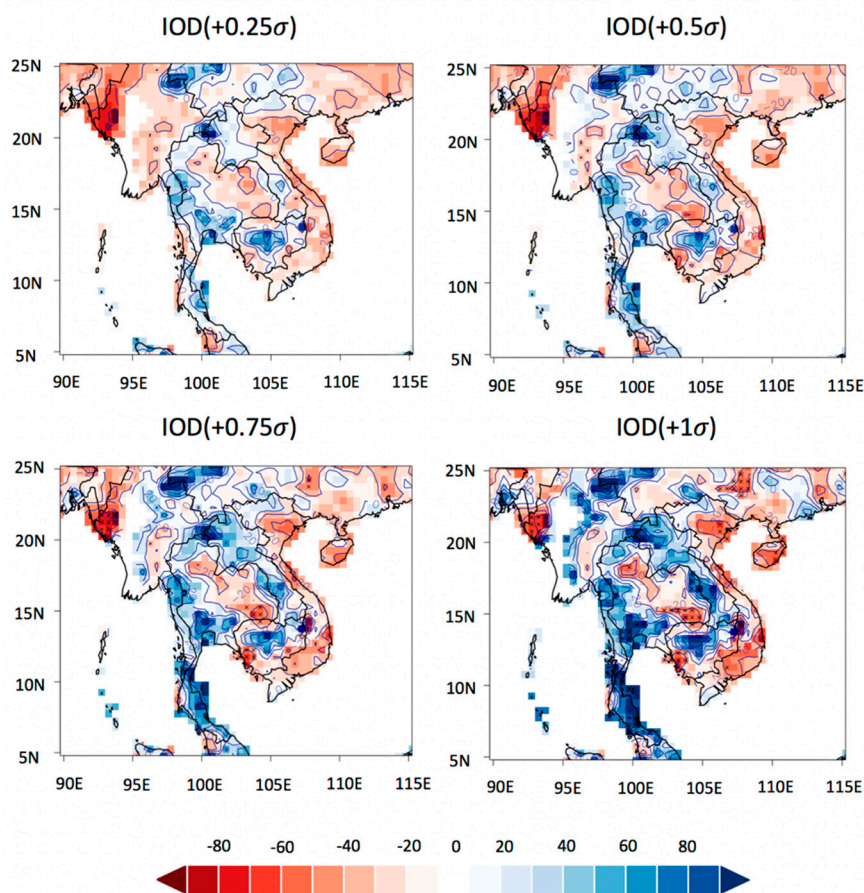


Figure 4. Percentage changes in extreme drought over the Indochina Peninsula (departures from the 1981–2010 norms). The climatology mean of IOD (1981–2010) was deliberately increased by 0.25σ through IBB simulations to analyze the sensitivity of extreme drought to the warming phase of IOD in the tropical Indian Ocean. In each figure, the median results derived from 1000 simulations are shown and the statistically significant area of change at 95% significance level is represented by “x”.

Figure 5 shows a 0.25σ decrease in the IOD. When negative IODs were strengthened, it was found that extreme droughts were less frequent throughout Laos, Vietnam, and the southwestern region of the Yunnan Province in China. However, in Northwestern Myanmar, some parts of Thailand, and in regions adjacent to the Andaman Sea, extreme drought increased, leading to greater drought vulnerability. In addition, IOD-sensitive areas with more extreme droughts emerged in the northwestern parts of

Myanmar, especially as changes in negative IOD became apparent. However, the eastern and northern parts of the ICP showed a contrasting response to negative IOD. The simulated results indicated that extreme droughts throughout Northwestern Myanmar and Thailand were more frequent than usual.

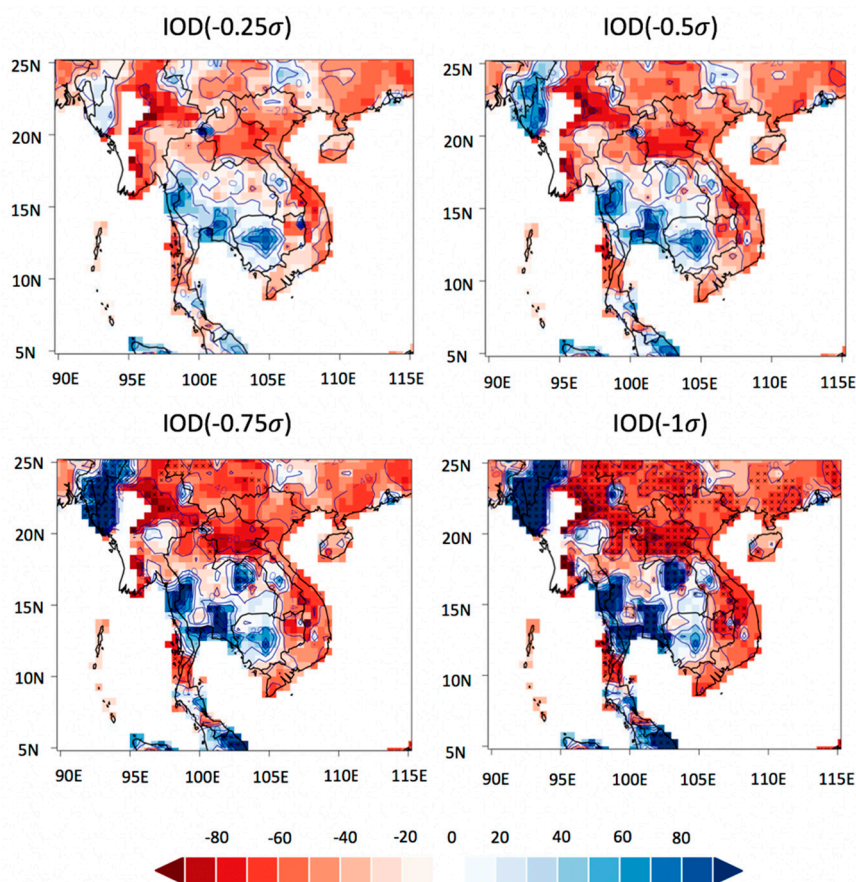


Figure 5. As Figure 4, but for a decrease in IOD in the tropical Indian Ocean.

4. Discussion and Conclusions

IOD in the Indian Ocean and ENSO in the Pacific Ocean are the results of atmospheric–ocean interactions in each region. Both phenomena can be identified by SST anomalies and are reported to have a direct impact on rainfall occurring globally [14,17,34–36]. The ENSO phenomenon has been officially observed since 1985 [37] and is relatively well known for its anomalous convection, wind patterns, and predictable short-term behaviors [38–41] within the global climate system. However, there is still a lack of understanding of interactions, evolutionary patterns, and predictability of new forms of El Niño [42].

Long-term drought conditions in Southeast Asia generally relate to El Niño, while wetter conditions tend to be associated with La Nina [43]. These changes are consistent with the results of the composite analysis of IOD and ENSO conducted in this study. When positive IOD and El Niño occur simultaneously, the spatial distribution of spring rainfall is significantly reduced compared to the rainfall anomaly pattern that takes into account positive IOD years only. Results for negative IOD years are similar to the changes observed for positive IOD years, but it is expanding to Northern Laos, Northeastern Myanmar, and Northern Thailand. These changes are more evident when the negative IOD years coincide with La Niña events.

Although different forms of El Niño have been reported to occur with increasing frequency in the central Pacific since the 2000s [36,40], the exact causes of these occurrences and their impacts on the Indian Ocean and Pacific Rim countries—according to the evolution patterns of different types

of El Niño events—are still unknown. Identification of different types of El Niño is evidence that ENSO events are not well understood and are certainly unpredictable [42]. Furthermore, ENSO and IOD–rainfall linkages in the ICP show significant spatial and seasonal variations. Recent studies suggested that the slowdown in the observed global average atmospheric temperature rise is closely related to substantial heat transfer from the Pacific Ocean to the Indian Ocean through Indonesian throughflow [44–46]. Despite similarities with ENSO, the IOD is an even more recent discovery with even less understood implications [14,18].

The spatio-temporal connection between SST and winds shows a strong coupling of precipitation and ocean dynamics in the Indian Ocean. However, with regards to the IOD phenomena, few quantitative studies provide a complete picture of extreme drought fluctuations across the ICP. Therefore, in this study, areas most vulnerable to drought were analyzed through statistical simulations of IODs using the IBB method based on historical observations.

The results of the long-term trend analysis show that the areas where spring rainfall has increased are mainly distributed along the eastern coast (Vietnam) and the northwestern portions of the ICP, while central and Northern Laos and Northern Cambodia have experienced a reduction in spring rainfall over the past few decades. This is because of the Truong-Son Mountains in Vietnam, which are adjacent to the South China Sea, have relatively abundant rainfall, whereas Laos has seen relatively little rainfall. This trend is similar to that of extreme droughts. Vietnam experienced less severe droughts, but central and Northern Laos suffered more severe droughts. During positive IOD years, extreme drought occurred less than usual throughout Vietnam and Southwestern China, while more droughts were observed in Cambodia and central Laos, as well as along the coastline adjacent to the Myanmar Sea. Results for negative IOD years are similar to changes observed for positive IOD years; however, the eastern and northern parts of the ICP are experiencing a decrease in droughts. In addition, the results of the statistical simulations proposed in this study successfully simulate drought-sensitive areas and evolution patterns for various IOD changes.

Investigating SST changes in the Indo-Pacific Ocean can help improve the understanding of regional-scale climatic variability as well as quantitatively diagnose this variability. Moreover, the sensitivity analysis of extreme drought to IODs based on the statistical simulations demonstrates the importance of further investigation of the mechanisms of IOD impacts on drought evolution in the ICP, which may include complex coupled oceanic–atmospheric processes. Although the results obtained herein were based on limited observations, the study’s findings have strong implications for improving extreme drought predictions in the ICP.

Author Contributions: conceptualization, J.-S.K.; Formal analysis, Q.-G.G. and J.-S.K.; Methodology, J.-H.L., V.S., and J.-S.K.; resources, V.S.; writing—original draft preparation, Q.-G.G. and J.-S.K.; writing—review and editing, L.X., J.-S.K., and J.-H.L.

Funding: This research is supported by the National Key R&D Program of China (2017YFC0405901), the National Natural Science Foundation of China (No. 51525902), and the Ministry of Education “111 Project” Fund of China (B18037), all of which are greatly appreciated. The fourth author was supported by Basic Science Research Program through the National Research Foundation of Korea (NRF) funded by the Ministry of Education (NRF-2017R1D1A1A02018546). The APC was funded by the National Key R&D Program of China (2017YFC0405901).

Conflicts of Interest: The authors declare no conflicts of interest.

References

1. Dai, A. Drought under global warming: A review. *Wiley Interdiscip. Rev. Clim. Change* **2011**, *2*, 45–65. [[CrossRef](#)]
2. Dai, A. Increasing drought under global warming in observations and models. *Nat. Clim. Change* **2013**, *3*, 52–58. [[CrossRef](#)]
3. Rind, D.; Goldberg, R.; Hansen, J.; Rosenzweig, C.; Ruedy, R. Potential evapotranspiration and the likelihood of future drought. *J. Geophys. Res.: Atmos.* **1990**, *95*, 9983–10004. [[CrossRef](#)]

4. Wang, G. Agricultural drought in a future climate: results from 15 global climate models participating in the IPCC 4th assessment. *Clim. Dyn.* **2005**, *25*, 739–753. [[CrossRef](#)]
5. Richard, R.; Heim, J. A Review of Twentieth-Century Drought Indices Used in the United States. *Bull. Am. Meteorol. Soc.* **2002**, *83*, 1149–1166.
6. Gao, Q.; Kim, J.-S.; Chen, J.; Chen, H.; Lee, J.-H. Atmospheric Teleconnection-Based Extreme Drought Prediction in the Core Drought Region in China. *Water* **2019**, *11*, 232. [[CrossRef](#)]
7. Le, M.H.; Perez, G.C.; Solomatine, D. Meteorological Drought Forecasting Based on Climate Signals Using Artificial Neural Network — A Case Study in Khanhhoa Province Vietnam. *Procedia Eng.* **2016**, *154*, 1169–1175. [[CrossRef](#)]
8. Nguyen, H.; Shaw, R. Chapter 8 Drought Risk Management in Vietnam. In *Droughts in Asian Monsoon Region*; Emerald Group Publishing Limited: Bingley, UK, 2011; pp. 141–161.
9. Hundertmark, W.J.I. Building drought management capacity in the Mekong river basin. *Irrig. Drain.* **2008**, *57*, 279–287. [[CrossRef](#)]
10. Vu, M.T.; Raghavan, V.S.; Liong, S.-Y. Ensemble Climate Projection for Hydro-Meteorological Drought over a river basin in Central Highland, Vietnam. *KSCE J. Civ. Eng.* **2015**, *19*, 427–433. [[CrossRef](#)]
11. Shu, F.; Prasoot, S.; Monthathip, C. Increasing Production of Rainfed Lowland Rice in Drought Prone Environments. *Plant Prod. Sci.* **1998**, *1*, 75–82.
12. Kim, J.-S.; Seo, G.-S.; Jang, H.-W.; Lee, J.-H. Correlation analysis between Korean spring drought and large-scale teleconnection patterns for drought forecasting. *KSCE J. Civ. Eng.* **2017**, *21*, 458–466. [[CrossRef](#)]
13. Zhang, Z.; Jin, Q.; Chen, X.; Xu, C.-Y.; Jiang, S.J. On the Linkage between the Extreme Drought and Pluvial Patterns in China and the Large-Scale Atmospheric Circulation. *Adv. Meteorol.* **2016**, *2016*. [[CrossRef](#)]
14. Saji, N.H.; Goswami, B.N.; Vinayachandran, P.N.; Yamagata, T. A dipole mode in the tropical Indian Ocean. *Nature* **1999**, *401*, 360–363. [[CrossRef](#)] [[PubMed](#)]
15. Jin, F.-F. An Equatorial Ocean Recharge Paradigm for ENSO. Part I: Conceptual Model. *J. Atmos. Sci.* **1997**, *54*, 811–829. [[CrossRef](#)]
16. Black, E.; Slingo, J.; Sperber, K.R. An Observational Study of the Relationship between Excessively Strong Short Rains in Coastal East Africa and Indian Ocean SST. *Mon. Weather Rev.* **2003**, *131*, 74–94. [[CrossRef](#)]
17. Ashok, K.; Guan, Z.; Yamagata, T. Impact of the Indian Ocean Dipole on the Relationship between the Indian Monsoon Rainfall and ENSO. *Geophys. Res. Lett.* **2001**, *28*, 4499–4502. [[CrossRef](#)]
18. Saji, N.; Yamagata, T. Possible impacts of Indian Ocean Dipole mode events on global climate. *Clim. Res.* **2003**, *25*, 151–169. [[CrossRef](#)]
19. Ashok, K.; Guan, Z.; Yamagata, T. Influence of the Indian Ocean Dipole on the Australian winter rainfall. *Geophys. Res. Lett.* **2003**, *30*, 1821. [[CrossRef](#)]
20. Liess, S.; Kumar, A.; Snyder, P.K.; Kawale, J.; Steinhäuser, K.; Semazzi, F.H.M.; Ganguly, A.R.; Samatova, N.F.; Kumar, V. Different Modes of Variability over the Tasman Sea: Implications for Regional Climate. *J. Clim.* **2014**, *27*, 8466–8486. [[CrossRef](#)]
21. Cai, W.; Cowan, T.; Sullivan, A. Recent unprecedented skewness towards positive Indian Ocean Dipole occurrences and its impact on Australian rainfall. *Geophys. Res. Lett.* **2009**, *36*, 245–253. [[CrossRef](#)]
22. Chan, S.C.; Behera, S.K.; Yamagata, T. Indian Ocean Dipole influence on South American rainfall. *Geophys. Res. Lett.* **2008**, *35*, L14S12. [[CrossRef](#)]
23. Zanchettin, D.; Bothe, O.; Müller, W.; Bader, J.; Jungclaus, J.H. Different flavors of the Atlantic Multidecadal Variability. *Clim. Dyn.* **2014**, *42*, 381–399. [[CrossRef](#)]
24. Cai, W.; Zheng, X.-T.; Weller, E.; Collins, M.; Cowan, T.; Lengaigne, M.; Yu, W.; Yamagata, T. Projected response of the Indian Ocean Dipole to greenhouse warming. *Nat. Geosci.* **2013**, *6*, 999–1007. [[CrossRef](#)]
25. Ihara, C.; Kushnir, Y.; Cane, M.A. Warming Trend of the Indian Ocean SST and Indian Ocean Dipole from 1880 to 2004. *J. Clim.* **2008**, *21*, 2035–2046. [[CrossRef](#)]
26. Ren, H.-L.; Jin, F.-F. Niño indices for two types of ENSO. *Geophys. Res. Lett.* **2011**, *38*. [[CrossRef](#)]
27. McKee, T.B.; Doesken, N.J.; Kleist, J. The relationship of drought frequency and duration to time scales. In Proceedings of the 8th Conference on Applied Climatology, 8th Conference on Applied Climatology, Anaheim, CA, USA, 17–22 January 1993; American Meteorological Society: Boston, MA, USA, 1993; pp. 179–183.
28. Guttman, N.B. ACCEPTING THE STANDARDIZED PRECIPITATION INDEX: A CALCULATION ALGORITHM. *J. Am. Water Resour. Assoc.* **1999**, *35*, 311–322. [[CrossRef](#)]

29. Mann, H.B. Nonparametric Tests Against Trend. *Econometrica* **1945**, *13*, 245–259. [[CrossRef](#)]
30. Kendall, M.G. *Rank correlation methods*; Griffin: Oxford, UK, 1948.
31. Hamed, K.H.; Rao, A.R. A modified Mann-Kendall trend test for autocorrelated data. *J. Hydrol.* **1998**, *204*, 182–196. [[CrossRef](#)]
32. Hall, P.; Presnell, B. Intentionally biased bootstrap methods. *J. R. Stat. Soc.* **1999**, *61*, 143–158. [[CrossRef](#)]
33. Lee, T. Climate change inspector with intentionally biased bootstrapping (CCIIBB ver. 1.0) — methodology development. *Geosci. Model Dev.* **2017**, *10*, 525–536. [[CrossRef](#)]
34. Piechota, T.C.; Chiew, F.H.S.; Dracup, J.A.; McMahon, T.A. Seasonal streamflow forecasting in eastern Australia and the El Niño–Southern Oscillation. *Water Resour. Res.* **1998**, *34*, 3035–3044. [[CrossRef](#)]
35. Mahala, B.K.; Nayak, B.K.; Mohanty, P.K. Impacts of ENSO and IOD on tropical cyclone activity in the Bay of Bengal. *Nat. Hazards* **2015**, *75*, 1105–1125. [[CrossRef](#)]
36. Pradhan, P.K.; Preethi, B.; Ashok, K.; Krishna, R.; Sahai, A.K. Modoki, Indian Ocean Dipole, and western North Pacific typhoons: Possible implications for extreme events. *J. Geophys. Res.* **2011**, *116*, D18108. [[CrossRef](#)]
37. McPhaden, M.J.; Ando, K.; Bourles, B.; Freitag, H.; Lumpkin, R.; Masumoto, Y.; Murty, V.; Nobre, P.; Ravichandran, M.; Vialard, J.J.P.O.O. The Global Tropical Moored Buoy Array. In Proceedings of the “OceanObs’09: Sustained Ocean Observations and Information for Society” Conference, OceanObs’09, Venice, Italy, 21–25 September 2009.
38. Kim, J.-S.; Son, C.-Y.; Moon, Y.-I.; Lee, J.-H. Seasonal rainfall variability in Korea within the context of different evolution patterns of the central Pacific El Niño. *J. Water Clim. Change* **2017**, *8*, 412–422. [[CrossRef](#)]
39. Kim, J.-S.; Kim, S.T.; Wang, L.; Wang, X.; Moon, Y.-I. Tropical cyclone activity in the northwestern Pacific associated with decaying Central Pacific El Niños. *Stochastic Environ. Res. Risk Assess.* **2016**, *30*, 1335–1345. [[CrossRef](#)]
40. Kim, J.-S.; Zhou, W.; Wang, X.; Jain, S. El Niño Modoki and the Summer Precipitation Variability over South Korea: A Diagnostic Study. *J. Meteorolog. Soc. Jpn.* **2012**, *90*, 673–684. [[CrossRef](#)]
41. Ashok, K.; Yamagata, T. Climate change: The El Niño with a difference. *Nature* **2009**, *461*, 481–484. [[CrossRef](#)] [[PubMed](#)]
42. Chiodi, A.M.; Harrison, D.E. Observed El Niño SSTA Development and the Effects of Easterly and Westerly Wind Events in 2014/15. *J. Clim.* **2017**, *30*, 1505–1519. [[CrossRef](#)]
43. Juneng, L.; Tangang, F.T. Evolution of ENSO-related rainfall anomalies in Southeast Asia region and its relationship with atmosphere–ocean variations in Indo-Pacific sector. *Clim. Dyn.* **2005**, *25*, 337–350. [[CrossRef](#)]
44. Kosaka, Y.; Xie, S.-P. Recent global-warming hiatus tied to equatorial Pacific surface cooling. *Nature* **2013**, *501*, 403. [[CrossRef](#)]
45. Lee, S.-K.; Park, W.; Baringer, M.O.; Gordon, A.L.; Huber, B.; Liu, Y. Pacific origin of the abrupt increase in Indian Ocean heat content during the warming hiatus. *Nat. Geosci.* **2015**, *8*, 445–449. [[CrossRef](#)]
46. Liu, W.; Xie, S.-P.; Lu, J. Tracking ocean heat uptake during the surface warming hiatus. *Nat. Commun.* **2016**, *7*, 10926. [[CrossRef](#)] [[PubMed](#)]

